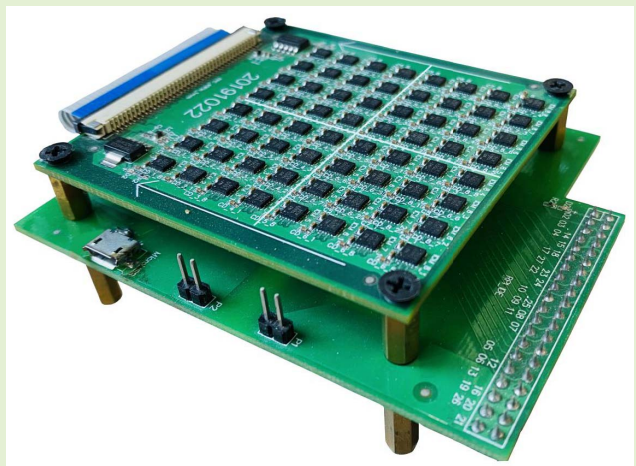


# Improving the Navigation Performance of the MEMS IMU Array by Precise Calibration

Liqiang Wang<sup>1</sup>, Hailiang Tang, Tisheng Zhang, Qijin Chen<sup>1</sup>, Jinwei Shi<sup>1</sup>, and Xiaoji Niu<sup>1</sup>

**Abstract**—Using a microelectromechanical system (MEMS) inertial measurement unit (IMU) array composed of multiple low-cost IMUs can reduce the measurement errors of inertial sensors, and improve its navigation performance. However, there is doubt about the benefit of the IMU array in the scene of GNSS/INS *dynamic navigation*. Therefore, to evaluate the navigation performance of the arrays, we developed four groups of IMU arrays, each containing 16 MEMS IMUs. Each IMU was accurately calibrated and compensated to improve the performance. The field experiments proved that the navigation accuracy of the IMU array improved by 3.4 times statistically over a single IMU, which is close to the theoretical limit, i.e., 4 times. Comparison data processing indicated that the individual IMU calibration reduced the horizontal position error of the array by 54% on average, which confirms that the precise calibration of each IMU, especially the cross-axis effect and mounting angles, is crucial to the array's navigation performance. This research provides firm experimental support for the application of IMU arrays in the field of navigation.

**Index Terms**—MEMS IMU, sensor array, IMU calibration, GNSS/INS.



## I. INTRODUCTION

**I**NERTIAL sensors, which are used to measure acceleration and angular velocity, have been studied since the discovery of the gyroscopic effect by Foucault in 1852 [1]. Since the 1950s, inertial sensors have been used in inertial navigation systems (INS). Until a few decades ago, they were limited to military and aerospace applications because of their bulkiness and high production costs. These drawbacks affected navigation-grade high-precision inertial devices such as the laser gyroscope. To overcome these challenges, microelectromechanical system (MEMS) inertial measurement unit (IMU) have been developed, which are advantageous in terms of their compactness and low cost [2], [3]. Thus IMUs are used in

civilian applications [4]. Currently, consumer-grade MEMS IMUs are widely used in the industry and civilian life, owing to their affordability and chip-level volume [5].

However, owing to their drawbacks concerning design principles and production processes, MEMS IMUs inevitably have larger measurement errors than laser-gyroscope-based IMUs; these errors lead to a large cumulative error when they are implemented in an INS. According to the random error theory, fusing multiple IMUs could yield more accurate and reliable inertial measurements [6]. Therefore, MEMS IMU arrays would significantly improve the inertial measurement accuracy, while remaining affordable. Consumer-grade MEMS IMUs (usually less than 1 US\$ per unit) can meet the low-cost and high-performance requirements of an IMU array.  $N$  inertial sensors with independent measurement errors expect that the uncertainty of measurement can be reduced by  $\sqrt{N}$  times after data fusion [7]. The IMU array's noise performance and potential for improving its navigation performance have drawn significant research interest.

Manuscript received June 21, 2021; accepted October 3, 2021. Date of publication October 6, 2021; date of current version November 12, 2021. This work was supported in part by the National Key Research and Development Program of China under Grant 2020YFB0505803 and in part by the National Natural Science Foundation of China under Grant 41974024. The associate editor coordinating the review of this article and approving it for publication was Dr. Ali Mohammadi. (*Corresponding author: Xiaoji Niu.*)

Liqiang Wang, Hailiang Tang, Tisheng Zhang, Qijin Chen, and Jinwei Shi are with the GNSS Research Center, Wuhan University, Wuhan 430079, China (e-mail: wlq@whu.edu.cn; thl@whu.edu.cn; zts@whu.edu.cn; chenqijin@whu.edu.cn; skingwei@whu.edu.cn).

Xiaoji Niu is with the GNSS Research Center, Wuhan University, Wuhan 430079, China, and also with the Artificial Intelligence Institute, Wuhan University, Wuhan 430079, China (e-mail: xjniu@whu.edu.cn).

Digital Object Identifier 10.1109/JSEN.2021.3118455

## A. Related Works

Recently, researchers have designed IMU arrays and evaluated the arrays' noise performance. For example, an IMU array comprising 16 MEMS IMUs was designed in [8], and the noise performance of the accelerometer and gyroscope containing in

the array was tested. The static noise root-mean-square (RMS) values of the accelerometer and gyroscope were reduced by 3.2 and 3.8 times, respectively. Nevertheless, the improvement effect of bias instability was slightly worse, which reduced by 2.8 and 3.0 times, respectively. The IMU array designed in [9] also contained 16 MEMS IMUs. The array was calibrated and compensated, and the data were fused using the mean filtering method. The gyroscope and accelerometer's bias instability errors were reduced by 4.02 and 3.51 times, respectively, and the angular/velocity random walk error was reduced by 3.89 and 3.67 times, respectively. As the IMU array was reinstalled once during the calibration process, the accelerometer's error improvement effect was a little worse. Additionally, the studies [10]–[13] designed IMU arrays that included 18, 5, and 32 IMUs, and the static noise performance of the arrays improved notably after data fusion.

In these studies, [9], [10], conducted the dynamic navigation experiment, but they did not achieve the expected performance improvement. Other studies on this topic were limited to investigating the static noise performance of the IMU array, while excluding dynamic errors (such as scale factor, cross-axis coupling, and the nonlinear errors).

Guerrier [14] designed a simulation model to validate the IMU array's navigation performance, and evaluated the performance enhancement after fusing 1–10 IMU data. The simulation results showed fusing the measurements of 10 IMUs could reduce the position error by approximately 40%, or increase the navigation performance by 2.5 times. Clausen *et al.* [15] assessed the navigation performance after fusing four IMU measurements through a vehicle field test. Their results showed that the IMU array's navigation error was smaller than that of a single IMU. However, they did not quantitatively evaluate the improvement in the navigation performance. Bancroft [16] calculated the dead reckoning of multiple independent IMU measurements, and added them to the Kalman estimator to obtain the positioning results. The fusing of 2, 3, 4, and 5 IMUs' measurements resulted in the error reductions of 25%, 29%, 32%, and 34%, respectively, and the navigation performance was enhanced by 1.30, 1.43, 1.47, and 1.51 times.

In [14], after fusing 10 IMUs, the navigation performance reached 79% of the theoretically predicted value. However, the simulation results can only be used as a reference because the dynamic sensor errors in the actual scene are ignored. The IMU array's navigation performance in [15] was improved to 67.5% of the theoretical value. However, they used an inadequate number of IMUs, which reduced the credibility of the results.

In the IMU array's data fusion algorithm, [8]–[13] took the average of the raw IMU observations as the fused measurement in noise performance evaluation. However, the articles [10], [11], [18] claimed that averaging was not the best method for dynamic data fusion, owing to the measurement errors (including scale factor and nonlinear errors) in dynamic experiments. The studies [14]–[16] did not directly perform measurement fusion on the raw IMU observations when evaluating the navigation performance. Instead, they fed the raw IMU observations or calculated motion information into the Kalman estimator, to solve the navigation information

along with the global navigation satellite system (GNSS) positioning result. Skog *et al.* [19] proposed a method based on maximum likelihood estimation for IMU array data fusion, and Schwaab *et al.* [20] employed the optimal linear unbiased estimation for the IMU array's measurement fusion. Although the methods worked in IMU array's data fusion, the dynamic experiments based on them did not yield the expected results. Martin *et al.* [17] designed three approaches that enhanced the measurement accuracy of IMU arrays. Although some sensors could benefit from the methods, they did not evaluate the improvement in terms of the IMU array's navigation performance.

The literature survey shows that the noise performance of an IMU array, which is composed of  $N$  IMUs, can be improved by a factor of approximately  $\sqrt{N}$  times, which is a theoretical value compared to a single IMU. However, the IMU arrays underperform in terms of dynamic navigation despite the available data fusion methods. Moreover, there has been a lack of dynamic navigation tests.

## B. Presented Work

We reason that the calibration and compensation to each individual IMU chip in an array, which was ignored in most cases in previous research, is of great importance and will significantly impact its dynamic navigation performance. Systematic errors such as scale factor and cross-axis coupling errors, introduce differences in each IMU's measurement result. The IMU chip's mounting angles on the array also disorients the three sensitive axes of each unit. These errors do not show up under stationary condition. However, under dynamic conditions (such as in a moving vehicle), the real values sensed by different IMU chips will be slightly deviated, which will cause the collected motion information to *blur* when the IMU array data are fused; consequently the measurement accuracy of the IMU array will reduce below the expected level. Hence, although the static noise performance of IMU arrays has significantly improved, the dynamic navigation performance rarely reach the desired improvement effect.

Based on these considerations, we designed an IMU array, and precisely calibrated the systematic error and mounting angles of each unit. Then, we compensated the raw IMU raw observation for the calibration parameters and size-effect. Finally, we fused the IMU array's measurements and evaluated its dynamic navigation performance. Moreover, to make the evaluation results representative and statistically significant, we fabricated four IMU arrays to obtain multisample test data. The calibration and dynamic experiment data used in this study were open-sourced which can be obtained on the website: <https://github.com/i2Nav-WHU/IMU-Array.git>.

## II. METHODOLOGY

We designed an IMU array, containing 16 MEMS IMU chips, a core processor, and data acquisition firmware. A special data reading method was employed to synchronously sample each IMU data. Then, the systematic errors and mounting angles of each IMU were calibrated and compensated with a high-precision turntable. Furthermore, the measurement of

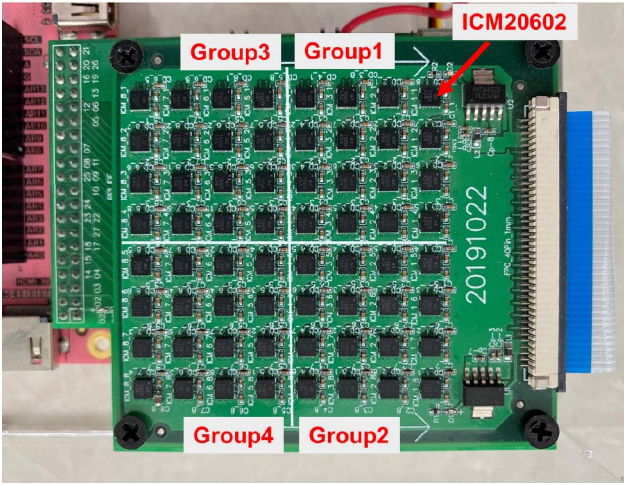


Fig. 1. Photograph of the designed IMU arrays.

each IMU was converted into the geometric center of the IMU array. The mounting angles and size-effect compensation of each individual IMU chip synchronized IMU's measurement spatially. Finally, data fusion was performed on every IMU's measurement, and the IMU array's noise performance was analyzed.

#### A. IMU Array Design

The number of the IMUs in the array is an important design consideration. An inadequate number of IMUs yields uncertain navigation performance because individual IMUs perform differently. Conversely, too many IMUs consume too much current from power supply, which cause the power ground unstable and generate additional measurement noise. Moreover, it would be difficult to simultaneously collect the IMU measurements if the array's scale were large. Accordingly, we selected 16 IMUs to construct the IMU array, to balance the accuracy of the performance evaluation and the data acquisition burden. This also ensured that minimal additional measurement noise resulted from the circuit power consumption disturbance.

A PYNQ-Z2 processor and 16 consumer-grade MEMS IMUs, ICM20602, were used in the IMU array. The low-noise power supply, isolation chip, and capacitor filter circuit were used in the array, to reduce the electrical noise and crosstalk among the chips. To more accurately test the improvement in the IMU array's navigation performance, we designed four groups of IMU arrays (Group 1–4) and soldered them to a single printed circuit board (PCB). A photograph of the IMU arrays is shown in Fig. 1.

A serial peripheral interface bus, including 16 parallel master-in slave-out ports [10], was used for data acquisition between the IMU array and PYNQ-Z2 processor, which synchronized the sampling time and data transmission of the 16 IMUs. The sampling rate of the IMU was set to 200 Hz (averaged from 1 KHz), which is sufficiently high for vehicle dynamics.

#### B. IMU Array Calibration

The IMU observation constitutes kinds of errors, each of which includes a constant part, random slow-changing part,

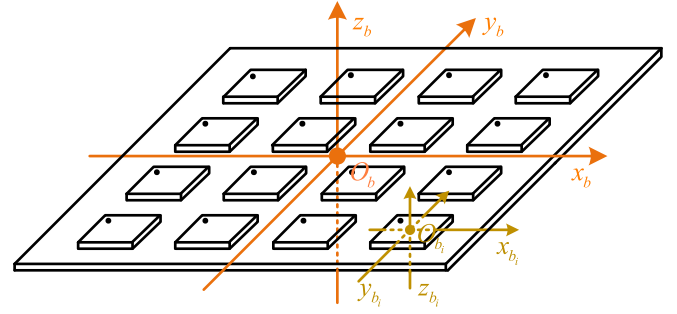


Fig. 2. IMU array's coordinate system.

and high-frequency noise part. The constant part, which is also called the systematic error, can be calibrated and compensated. The random slow-changing and the high-frequency noise parts are known as random errors. Each IMU in the array has different mounting angles, yielding varying measurements. It is expected that the measurement obtained by each IMU deviates only because of random errors when the measurement values are combined. Therefore, only the systematic error and mounting angles of each IMU were compensated well, more accurate inertial measurement values can be obtained after the data fusion.

When calibrating the IMUs, we marked the coordinate systems of each IMU as the  $b_i$  frame, where  $i = 1, 2, \dots, 16$ . The origin of the frame is the geometric center of each IMU chip. The IMU array coordinate system was marked as the  $b$  frame—the origin of which is the IMU array's geometric center. The schematic of the coordinate system is illustrated in Fig. 2.

1) *IMU Array Calibration Model*: By considering the systematic errors in the raw IMU observation, we established the measurement model of the gyroscope in the  $i$ -th IMU can follows [21], [22].

$$\tilde{\omega}^{b_i} = (\mathbf{I} + \mathbf{S}_{gi} + \mathbf{N}_{gi})\omega^{b_i} + \mathbf{b}_{gi} + \mathbf{v}_{gi}, \quad (1)$$

where  $\omega^{b_i}$  is the true angular velocity of the gyroscope in the  $i$ -th IMU;  $\tilde{\omega}^{b_i}$  is the angular velocity measured by the gyroscope;  $\mathbf{v}_{gi}$  represents the measurement noise; and  $\mathbf{S}_{gi}$ ,  $\mathbf{N}_{gi}$ , and  $\mathbf{b}_{gi}$  are the systematic errors, representing the gyroscope's scale factor error, cross-coupling error, and the constant zero offsets, respectively.

During the calibration, the PCB of the IMU array was mounted on and aligned with a precision turntable, such that only the angular velocity in the  $b$  frame could be accurately known, whereas the actual input in the  $b_i$  frame could not be determined. Therefore, the mounting angles—the angles between the three axes of the  $b_i$  and  $b$  frames, must be considered during the calibration. Thus, the model was expressed as

$$\tilde{\omega}^{b_i} = (\mathbf{I} + \mathbf{S}_{gi} + \mathbf{N}_{gi})\mathbf{C}_b^{b_i}\omega^b + \mathbf{b}_{gi} + \mathbf{v}_{gi}, \quad (2)$$

where  $\omega^b$  is the true angular velocity of the IMU array, and  $\mathbf{C}_b^{b_i}$  is the rotation matrix between the  $b$  and  $b_i$  frames.

Similarly, the  $i$ -th accelerometer's measurement model was constructed as

$$\tilde{\mathbf{f}}^{b_i} = (\mathbf{I} + \mathbf{S}_{ai} + \mathbf{N}_{ai})\mathbf{C}_b^{b_i}\mathbf{f}^b + \mathbf{b}_{ai} + \mathbf{v}_{ai}, \quad (3)$$

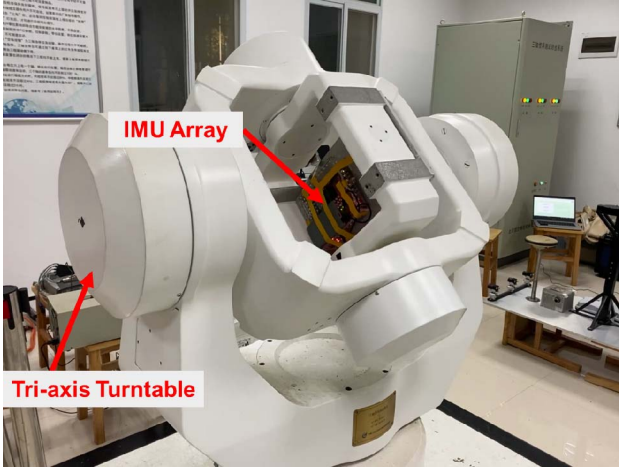


Fig. 3. IMU array calibration on the turntable.

where  $f^b$  is the input specific force of the IMU array;  $\tilde{f}^{b_i}$  represents the specific force measured by the accelerometer;  $v_{ai}$  is the measurement noise; and  $S_{ai}$ ,  $N_{ai}$ , and  $b_{ai}$  are the scale factor error, cross-axis coupling error, and constant zero offsets, respectively.

Let  $K_{gi} = (I + S_{gi} + N_{gi})C_b^{b_i}$  and  $K_{ai} = (I + S_{ai} + N_{ai})C_b^{b_i}$ , then we can calibrate the gyroscope and accelerometer through the angle position method and the six-position method, respectively [23], [24].

**2) IMU Array Calibration Process:** The high-precision turntable shown in Fig. 3 was used to calibrate each IMU in the array. First, the array was aligned along the rotational axes of the turntable and mounted on it. Then the gyroscope and accelerometer were calibrated.

When calibrated the gyroscope, we rotated the turntable so that the three axes of the array were vertically upward in turn. Each axis rotated clockwise and counterclockwise for four full circles, i.e.,  $1,440^\circ$ . At the beginning and end, the table was accelerated and decelerated with an angular acceleration of  $5 \text{ deg/s}^2$ , and rotated during the middle time at a constant  $30 \text{ deg/s}$ , which is a typical angular velocity in vehicle movement.

During the gyroscope's calibration, the earth's rotational angular velocity has a stable component along the rotational axis, and a time-varying sinusoidal component along the two horizontal axes. We considered the entire rotation process to be uniform. Thus, the angles of rotation along the two horizontal axes equal zero after integration. The angle measured by the vertical axis within  $t$  s can be obtained through integral calculation, which can be expressed as

$$\alpha = \alpha_{table} + \omega_e \sin(\phi)t, \quad (4)$$

where  $\alpha_{table} = 1,440^\circ$  is the rotation angle of the turntable,  $\omega_e$  is the earth's rate of rotation and  $\phi$  donates the local latitude.

By integrating the angular velocity from the gyroscope as the observation vector, we solved the parameter matrix and stable bias error using the least square method [25].

While calibrating the accelerometer, we rotated the table so that each axis of the IMU array was vertically upward and downward, respectively. Static data were collected at each position for 2 min, which reduced the influence of measure-

ment noise on the calibration results and fluctuations in the observations caused by the bias instability. By considering the local gravity as the real input specific force of the accelerometer and the average of the accelerometer's measurement as the observation vector, we solved the unknown parameter using the least square method [25].

### C. IMU Array Measurement Fusion

**1) Size-Effect Compensation:** The mounting angles of each IMU on the array were considered in the calibration process. Before fusing the IMU array's data, it is necessary to convert the inertial measurements into the same spatial position, i.e., to compensate for the size effect of each IMU. The size-effect compensation converts the measurement of the IMU from the  $b_i$  to  $b$  frame.

The IMU array is a rigid body, thus, all positions on the PCB have the same angular velocity. The angular velocity after the size-effect compensation was  $\tilde{\omega}_i^b = \tilde{\omega}^{b_i}$ , where  $\tilde{\omega}^{b_i}$  is the angular velocity after compensation for the calibration parameter.

Basic kinematics dictate that the specific force at one point on a rotating coordinate frame can be decomposed into that at another point, a centrifugal term, and an Eulerian term [26]. Therefore, the specific force of the  $i$ -th IMU after the size-effect compensation was expressed as

$$\tilde{f}_i^{b_i} = \tilde{f}^{b_i} - \omega_i^b \times (\omega_i^b \times r_i) - \dot{\omega}_i^b \times r_i \quad (5)$$

where  $\tilde{f}^{b_i}$  is the specific force after compensation for the calibration parameter;  $\omega_i^b$  and  $\dot{\omega}_i^b$  are the angular velocity and angular acceleration of the IMU array, respectively; and  $r_i$  is the IMU's position in the  $b$  frame, which was accurately set in the PCB design.

**2) Measurement Fusion:** The random error of an IMU is critical to maintaining the accuracy of the GNSS/INS integrated navigation system. The IMU array reduces the high-frequency noise and random slow-changing error via measurement fusion. Consequently, the navigation accuracy of the IMU array is improved. This study fuses data of the IMU array at the sensor level [27]. That is, the measurement of each IMU is firstly fused to obtain the IMU array's inertial data. The fused measurement is then used in the GNSS/INS integrated navigation system.

Although utilizing the mean value yields suboptimal performance [18], it also effectively reduces the measurement noise if all IMUs exhibit equivalent noise performance. Moreover, this approach is less computationally taxing and easier to implement in engineering than the least square estimator [28]. Therefore, this study considers the average of the measurements for data fusion. The measurement noise of the IMU array can be calculated as follows [7], [8].

$$v_A = \frac{1}{N} \sum_{i=1}^N v_{ai} \quad \sigma_a^2 = E[(v_{ai})^2], \quad (6)$$

$$\sigma_A^2 = E\left[\left(\frac{1}{N} \sum_{i=1}^N v_{ai}\right)^2\right] = \frac{1}{N^2} E\left[\sum_{i=1}^N (v_{ai})^2\right] = \frac{1}{N} \sigma_{ai}^2, \quad (7)$$

TABLE I  
NOISE PERFORMANCE IMPROVEMENT OF IMU ARRAYS

Improvement Ratio	Gyroscope		Accelerometer	
	Random Walk	Bias Instability	Random Walk	Bias Instability
Group1	3.73	3.41	3.96	3.43
Group2	3.77	3.49	3.95	3.32
Group3	3.94	3.59	3.95	3.43
Group4	3.98	3.46	3.98	3.73
Average	3.86	3.49	3.96	3.48
	3.67		3.72	

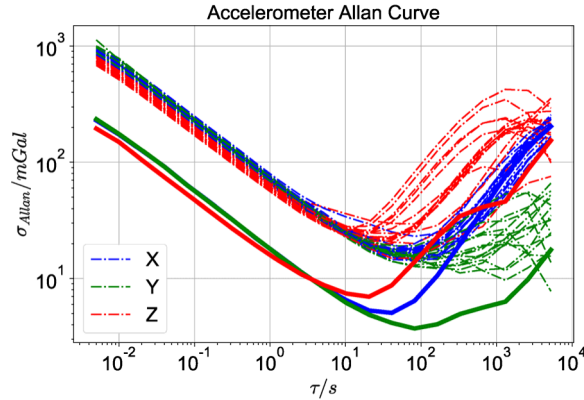


Fig. 4. Accelerometers' allan variance plot of IMU array (group 3 as example).

where  $v_{ai}$  is the zero-mean noise of a single IMU,  $\sigma_a^2$  is the noise variance,  $v_A$  is the measurement noise of the IMU array, and  $\sigma_A^2$  its noise variance.

Notably, the standard deviation of the IMU array measurement noise will be theoretically reduced by  $\sqrt{N}$  times than that of a single IMU. That is, under ideal circumstances, the performance of the IMU array can be increased by  $\sqrt{N}$  times.

3) *IMU Array's Noise Performance*: Angle (velocity) random walk (ARW or VRW) and in-run bias instability in random error are crucial indicators of the noise performance of an IMU array. Allan variance—a common method for analyzing and quantifying the random error of inertial sensors currently—is used to quantitatively evaluate the ARW/VRW and bias instability of the IMU array. The random error term in the inertial sensor's static data can be clearly expressed in the Allan variance plot, and the error coefficient can be obtained through a simple calculation [29].

To evaluate their static performance, 8 h of static data were collected from the 4 IMU arrays on the stable turntable at a relatively stable temperature. The Allan variance plots of the accelerometers of the third IMU array are illustrated in Fig. 4. Each dash-dotted line in the figure is the Allan variance plot of the individual IMU, whereas the thick solid lines denote the array's Allan plots. The Allan curve of the IMU array gyroscope yields a similar trend. Then, the random error coefficient was calculated, and the average of 16 IMU coefficients was considered as the error coefficient of a single IMU. The improvement in the IMU array's noise performance was gauged by comparing the random error coefficient of a

single IMU with that of the array. The average improvement ratio of the ARW and the bias instability of the gyroscope is considered as the performance improvement of the IMU array's gyroscope. The accelerometer's performance is defined similarly. The improvement ratios of the four IMU arrays' noise performance are listed in Table I.

The noise performance of the four arrays demonstrated significant improvement over that of a single IMU. The average improvement ratios of the gyroscope and accelerometer were 3.67 and 3.72 times, respectively. That is, the IMU array's noise performance increased by 3.70 times on average, which is close to the theoretical factor of 4. It also proved that the noise performance of the designed four IMU arrays improved nearly ideally.

### III. EXPERIMENTS AND DISCUSSION

To accurately evaluate the improvement in the IMU array's dynamic navigation performance, we performed field experiments on the four groups of IMU arrays. The navigation performance and impact of calibration and compensation on the four groups will be discussed in this section.

#### A. Experiment Description

The experiment was carried out on a terrestrial vehicle. Fig. 5 shows a photograph of the vehicle and experimental setups. In this test, the IMU array, an integrated navigation module, INS-Probe, and a navigation-grade GNSS/INS Ledor-A15 were used. The INS-Probe was used to synchronize the data of each IMU with the GNSS time. The positioning result of Ledor-A15 served as the ground truth. To acquire a high-precision GNSS positioning result, the raw GNSS observations of the rover (test vehicle) and nearby base station were preserved and used for post-processed kinematic (PPK).

Fig. 6 illustrates the driving track of the vehicle in a full open-sky condition. The open experimental area ensured the acquisition of centimeter-level GNSS positioning, which provided more accurate reference trajectories and reduced the influence of the GNSS positioning error on the performance evaluation of the IMU array. The experimental setups were activated, and the vehicle was stationary for 400 s, such that Ledor-A15 could perform static alignment. Subsequently, the vehicle was driven along the complex trajectory shown in the figure, and accelerated and decelerated to expedite the convergence of various errors in the integrated navigation

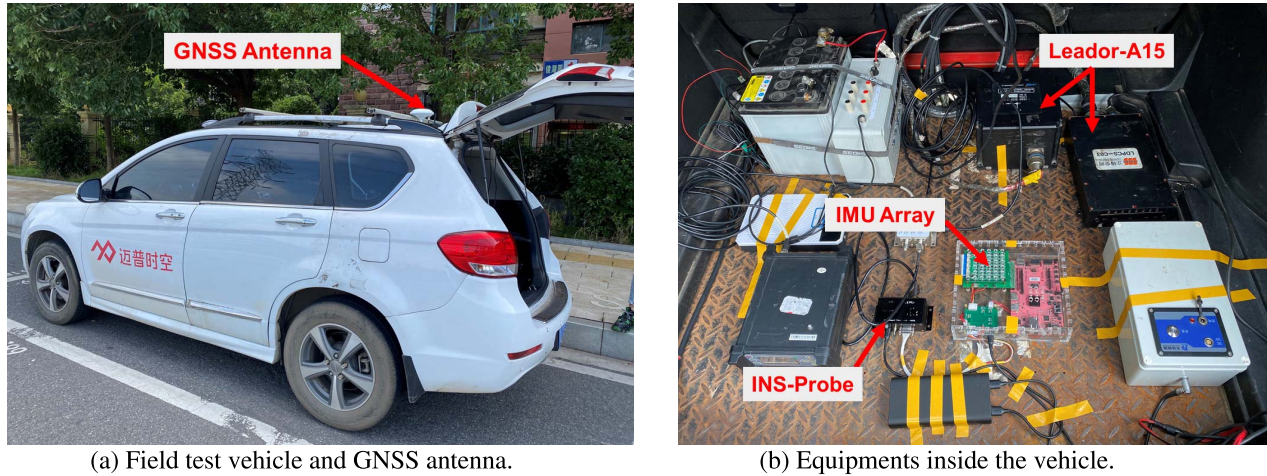


Fig. 5. Experimental setups of the field test.



Fig. 6. Trajectory of the dynamic navigation test.

system. The four IMU arrays were tested at this location for more than 40 min.

### B. Data Processing Method

The dynamic navigation performance of the IMU arrays was compared using the data processing diagram shown in Fig. 7.

First, centimeter-level GNSS positioning results were obtained by performing PPK operations on the GNSS raw observations of the rover and base station. The millimeter-level positioning result of Leador-A15, which served as the reference trajectory, was acquired using the Rauch-Tung-Striebel smoother.

Then the positioning result of each IMU and the array were calculated using the extended Kalman filter (EKF). The error parameters in the EKF of a single IMU chip and the IMU array were optimized separately. GNSS outage, which were introduced to evaluate the navigation performance of the IMU array, occurred after the vehicle moved for 400 s. The outage length and interval were 30 and 90 s, respectively. The gyroscope measurements when the vehicle was stationary were performed as the initial bias error in the EKF, such that the state errors converged expeditiously.

Next, the positioning errors of a single IMU and the array were acquired by comparing their positioning results with the

reference trajectory. Then, we calculated the RMS value of the maximum position error during all periods of outage, and recorded it as the positioning error of the array. The same method was used for each IMU's positioning error, and the RMS value of the positioning errors of all 16 IMUs was considered as the positioning error of a single IMU.

To more accurately evaluate the positioning error of the IMU array, we postponed all periods of the GNSS outage by 30 and 60s. Thus, the GNSS outage time covered the entire test period, retrieving more navigation error samples. The computation was repeated to acquire the positioning error.

Finally, the improvement in the navigation performance of the IMU array was gauged by comparing the positioning errors of the IMU array and a single IMU.

It is worth mentioning that the InvenSense's MEMS IMU, ICM20602, produced low-frequency noise in the z-axis measurement of the accelerometer in a static state; i.e., the z-axis Allan curve bulges before fully reaching the bottom (Fig. 4). Another MEMS IMU from InvenSense, MPU6000, was used in a previous study to evaluate the noise performance of an IMU array [9]. The same phenomenon also appears on the accelerometer's Allan curve. The common low-frequency noise in the accelerometer's z-axis severely affects the performance along the IMU array's z-axis. Therefore, when evaluating the IMU array's navigation performance, we judged the navigation accuracy based on the horizontal position error, without considering the altitude error.

### C. Navigation Performance Improvement

The four IMU arrays' positioning errors were calculated using the processing method. The error drift curve of the first IMU array is illustrated in Fig. 8. In this graph, the positioning error was calculated from 29 GNSS outage test samples. That is, approximately 90 GNSS outage samples were used to evaluate the navigation performance of each IMU and the array. This raised the accuracy and credibility of the improvement evaluation. The horizontal position errors of the four IMU arrays and a single IMU at different outage start times are shown in Table II.

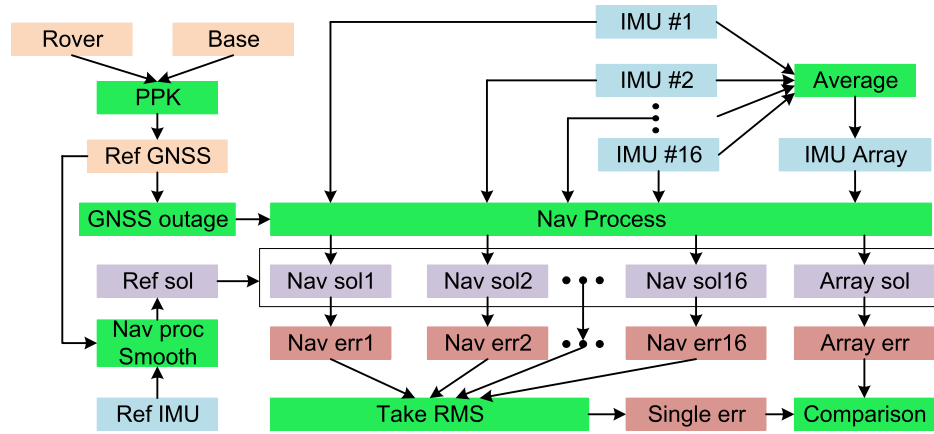


Fig. 7. Field test data processing and analysis block diagram.

TABLE II  
HORIZONTAL POSITION ERROR OF THE FOUR IMU ARRAYS IN THREE GNSS OUTAGE TESTS

IMU Array	Outage Start Time	30s GNSS Outage Horizontal Error (RMS)/m		Ratio
		Single IMU	IMU Array	
Group1	$t_{start} + 400s$	6.49	2.06	3.15
	$t_{start} + 430s$	6.43	1.85	3.47
	$t_{start} + 460s$	6.39	1.85	3.45
	<b>RMS</b>	<b>6.44</b>	<b>1.92</b>	<b>3.35</b>
Group2	$t_{start} + 400s$	8.12	1.85	4.39
	$t_{start} + 430s$	5.63	2.04	2.76
	$t_{start} + 460s$	6.17	1.92	3.22
	<b>RMS</b>	<b>6.73</b>	<b>1.94</b>	<b>3.47</b>
Group3	$t_{start} + 400s$	6.50	1.44	4.53
	$t_{start} + 430s$	5.78	1.76	3.29
	$t_{start} + 460s$	5.60	1.89	2.96
	<b>RMS</b>	<b>5.97</b>	<b>1.71</b>	<b>3.50</b>
Group4	$t_{start} + 400s$	5.36	1.67	3.21
	$t_{start} + 430s$	5.82	2.04	2.85
	$t_{start} + 460s$	6.24	1.73	3.61
	<b>RMS</b>	<b>5.82</b>	<b>1.82</b>	<b>3.19</b>
Average	<b>RMS</b>	<b>6.24</b>	<b>1.85</b>	<b>3.38</b>

According to Table II, the horizontal position errors of the four IMU arrays significantly reduced for the three different outage tests compared to that of a single IMU. However, the improvement effect of the IMU array's position error varied by group in the outage tests. Specifically, the position error of Group2 reduced 4.39 times in the first outage test, and 2.76 times in the second test. This difference is related to the random test situation, including the GNSS positioning error and vehicle's dynamics. It also reflects the significance of increasing the number of outage test samples, as it distributes the GNSS outage period throughout the entire test process and helps more accurately reflect the IMU's navigation performance in terms of the position error.

The RMS value of the horizontal position error in the three different outage tests was calculated. The ratio of the RMS of a single IMU's horizontal position error to that of the IMU array was considered as the improvement effect

in the array's navigation performance. However, the degree of improvement was different for the four IMU arrays. The extent of improvements in Group 1–3 were similar, i.e., approximately 3.4 times, whereas that in Group 4 reduced by 3.19 times. This was attributed to the individual differences in the navigation performance of the IMUs and vehicle's dynamics.

Despite the influence of the test conditions and individual differences, the average position error of the four IMU arrays reduced 3.38 times over a single IMU, which is close to the theoretical factor of 4. Considering that the measurement errors of the IMUs were not entirely independent of one another, it can be determined that after precise calibration and compensation, the four IMU arrays achieved the desired performance improvement. These results led us to conclude that *the dynamic navigation performance of an IMU array comprising 16 MEMS IMU chips improves by nearly 4 times.*

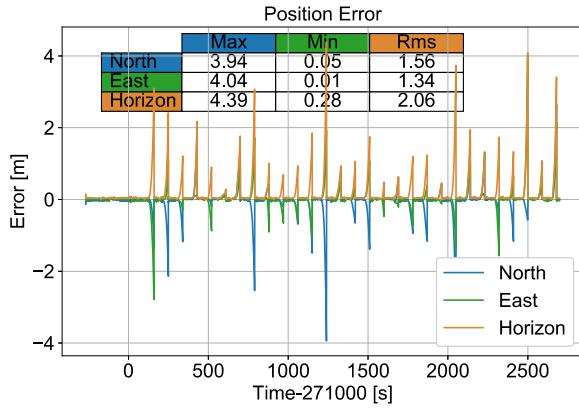


Fig. 8. Position error of IMU array (group 1 as example).

TABLE III  
HORIZONTAL POSITION ERROR OF THE IMU ARRAY BEFORE CALIBRATION AND COMPENSATION

Array	Horizontal Position Error(RMS)/m		Ratio
	Single IMU	IMU Array	
Group1	6.19	4.90	1.26
Group2	6.68	3.03	2.21
Group3	6.17	3.87	1.59
Group4	5.97	5.11	1.17
Average	6.25	4.23	1.56

#### D. Impact of Calibration and Compensation

The calibration and compensation of each individual IMU in the array played an essential role in improving its dynamic navigation performance. However, no published results on the effect of calibration and compensation on the IMU array's performance improvement exist. Therefore, to confirm the observation, we tested the array's navigation performance before and after the calibration and compensation. We fused data on the measurement values of each IMU that were not compensated for the calibration parameters, and applied data processing method (from Section III.B) to calculate the navigation position error. The horizontal position error and error reduction ratio of the four IMU arrays before calibration and compensation are listed in Table III.

In Table III, the array's position error before the compensation improved by only 1.56 times on average, which is far from the desired effect. The horizontal position error of a single IMU in Table III before and after the calibration and compensation are almost the same as those in Table II, whereas the IMU arrays' position errors are significantly different. This confirms that compensating the systematic errors and mounting angles effectively suppressed the motion information blur in the IMU array's data fusion.

The position errors of the four IMU arrays after the calibration and compensation reduced by 61 %, 36 %, 56 %, and 64 %. The degree of reduction varies with the array because each IMU had a different systematic error and mounting angles. Furthermore, the difference between the test dynamics of the four arrays caused arbitrary error reductions after the compensation. Nonetheless, the four groups of test results showed a significant reduction in the position error of the IMU array after the calibration and compensation, with an

average reduction of 54 %. We conclude that *the calibration and compensation of each individual IMU effectively improves the measurement accuracy of the IMU array.*

We reproduced the same test on a low-speed wheeled robot with a maximum speed of 1.5 m/s. However, in the robot test, the calibration and compensation of the individual IMU did not significantly influence the array's navigation performance.

The test and analysis results led us to infer that *when the dynamics of the IMU array are higher, the significance of the calibration and compensation are greater.* This conclusion could explain the problem expressed in previous studies (such as [9], [10]) that the static performance of the IMU array had improved significantly, while the dynamic navigation performance had not reached the ideal effect.

In this study, the IMU array with 16 IMU chips achieved an effect close to the theoretical value. In future studies, each IMU must be more precisely calibrated (mostly the cross-axis coupling error and mounting angles) if higher navigation accuracy is expected by increasing the array size. However, for the MEMS IMU chips, which have few stable parameters, the precision of calibration may not be guaranteed. Therefore, improving the navigation performance by solely increasing the scale of the IMU array should be studied further.

#### IV. CONCLUSION

This study enhanced the dynamic navigation performance of an IMU array by precise calibration and verified the improvement of the IMU array through field tests firmly. The results showed an improvement of 3.7 times on average in terms of the noise performance of the arrays. The vehicle's dynamic navigation performance with integrated GNSS/INS was improved by 3.4 times. Both the static sensor errors and the dynamic navigation performances improved by a factor close to the theoretical one, i.e., 4 times. The results also demonstrated the importance of calibrating and compensating each IMU in terms of the dynamic navigation performance of the array. The dynamic navigation error was reduced by 54 % on average after the calibration and compensation.

The self-calibration of an IMU array [30] is more affordable and feasible than the calibration using a high-precision turntable. Therefore, future work shall focus on a simple, yet effective, method to calibrate the IMU arrays in a systematic way.

#### ACKNOWLEDGMENT

The authors would like to thank Wanwei Zhang, who is a Laboratory Technician at the School of Geodesy and Geomatics, Wuhan University, for assisting them with the turntable calibration.

#### REFERENCES

- [1] D. Titterton, J. L. Weston, and J. Weston, *Strapdown Inertial Navigation Technology*. London, U.K.: The Institution of Electrical Engineers, 2004.
- [2] G. Zhanshe, C. Fucheng, L. Boyu, C. Le, L. Chao, and S. Ke, "Research development of silicon MEMS gyroscopes: A review," *Microsyst. Technol.*, vol. 21, no. 10, pp. 2053–2066, Oct. 2015.
- [3] N. Yazdi, F. Ayazi, and K. Najafi, "Micromachined inertial sensors," *Proc. IEEE*, vol. 86, no. 8, pp. 1640–1659, Aug. 1998.
- [4] N. Ahmad, R. A. R. Ghazilla, N. M. Khairi, and V. Kasi, "Reviews on various inertial measurement unit (IMU) sensor applications," *Int. J. Signal Process. Syst.*, vol. 1, no. 2, pp. 256–262, 2013.

- [5] N. El-Sheimy and A. Youssef, "Inertial sensors technologies for navigation applications: State of the art and future trends," *Satell. Navigat.*, vol. 1, no. 1, pp. 1–21, Dec. 2020.
- [6] J.-O. Nilsson and I. Skog, "Inertial sensor arrays—A literature review," in *Proc. Eur. Navigat. Conf. (ENC)*, May/June 2016, pp. 1–10.
- [7] R. G. Brown and P. Y. C. Hwang, *Introduction to Random Signals and Applied Kalman Filtering With MATLAB Exercises*, 4th ed. Hoboken, NJ, USA: Wiley, 2012.
- [8] D. Greenheck, R. Bishop, E. Jonardi, and J. Christian, "Design and testing of a low-cost MEMS IMU cluster for smallsat applications," in *Proc. Small Satell. Conf.*, Aug. 2014, pp. 1–24.
- [9] D. R. Greenheck, "Design and characterization of a low cost MEMS IMU cluster for precision navigation," M.S. thesis, Dept. Elect. Eng., Marquette Univ., Milwaukee, Wisconsin, 2015.
- [10] I. Skog, J.-O. Nilsson, and P. Händel, "An open-source multi inertial measurement unit (MIMU) platform," in *Proc. Int. Symp. Inertial Sensors Syst. (ISISS)*, Feb. 2014, pp. 1–4.
- [11] A. P. Moschevikin, A. Sikora, P. V. Lunkov, A. A. Fedorov, and E. I. Maslennikov, "Hardware and software architecture of multi MEMS sensor inertial module," in *Proc. 24th Saint Petersburg Int. Conf. Integr. Navigat. Syst. (ICINS)*, May 2017, pp. 1–3.
- [12] S. Bose, A. K. Gupta, and P. Handel, "On the noise and power performance of a shoe-mounted multi-IMU inertial positioning system," in *Proc. Int. Conf. Indoor Positioning Indoor Navigat. (IPIN)*, Sep. 2017, pp. 1–8.
- [13] T. Jing and H. Zhao, "Research on array MEMS inertial sensor and noise suppression," *Chin. J. Sens. Actuators*, vol. 33, no. 6, pp. 779–784, 2020.
- [14] S. Guerrier, "Improving accuracy with multiple sensors: Study of redundant MEMS-IMU/GPS configurations," in *Proc. 22nd Int. Tech. Meeting Satell. Division Inst. Navigat. (ION GNSS)*, 2009, pp. 3114–3121.
- [15] P. Clausen *et al.*, "Position accuracy with redundant MEMS IMU for road applications," *Eur. J. Navigat.*, vol. 13, no. 2, pp. 4–12, 2015.
- [16] J. B. Bancroft, "Multiple IMU integration for vehicular navigation," in *Proc. 22nd Int. Tech. Meeting Satell. Division Inst. Navigat. (ION GNSS)*, 2009, pp. 1828–1840.
- [17] H. Martin, P. Groves, M. Newman, and R. Faragher, "A new approach to better low-cost MEMS IMU performance using sensor arrays," in *Proc. 26th Int. Tech. Meeting Satell. Division The Inst. Navigat. (ION GNSS+)*, 2013, pp. 2125–2142.
- [18] I. Skog, J.-O. Nilsson, and P. Handel, "Pedestrian tracking using an IMU array," in *Proc. IEEE Int. Conf. Electron., Comput. Commun. Technol. (CONECCT)*, Jan. 2014, pp. 1–4.
- [19] I. Skog, J.-O. Nilsson, P. Handel, and A. Nehorai, "Inertial sensor arrays, maximum likelihood, and Cramér–Rao bound," *IEEE Trans. Signal Process.*, vol. 64, no. 16, pp. 4218–4227, Aug. 2016.
- [20] M. Schwaab, S. A. Regina, A. Sikora, and E. V. Abramov, "Measurement analysis of multiple MEMS sensor array," in *Proc. 24th Saint Petersburg Int. Conf. Integr. Navigat. Syst. (ICINS)*, May 2017, pp. 1–4.
- [21] R. Zhang, F. Höflinger, and L. M. Reind, "Calibration of an IMU using 3-D rotation platform," *IEEE Sensors J.*, vol. 14, no. 6, pp. 1778–1787, Jun. 2014.
- [22] U. Qureshi and F. Golnaraghi, "An algorithm for the in-field calibration of a MEMS IMU," *IEEE Sensors J.*, vol. 17, no. 22, pp. 7479–7486, Nov. 2017.
- [23] M. El-Diasty and S. Pagiatakis, "Calibration and stochastic modelling of inertial navigation sensor errors," *J. Global Positioning Syst.*, vol. 7, no. 2, pp. 170–182, 2008.
- [24] Z. F. Syed, P. Aggarwal, C. Goodall, X. Niu, and N. El-Sheimy, "A new multi-position calibration method for MEMS inertial navigation systems," *Meas. Sci. Technol.*, vol. 18, no. 7, p. 1897, 2007.
- [25] Å. Björck, *Least Squares Methods*. North-Holland: Handbook of Numerical Analysis, 1990.
- [26] T. R. Kane and D. A. Levinson, *Dynamics—Theory and Applications*. Ithaca, NY, USA: The Internet-First Univ. Press, 2005.
- [27] A. Waegli, S. Guerrier, and J. Skaloud, "Redundant MEMS-IMU integrated with GPS for performance assessment in sports," in *Proc. IEEE/ION PLANS*, May 2008, pp. 1260–1268.
- [28] J. B. Bancroft and G. Lachapelle, "Data fusion algorithms for multiple inertial measurement units," *Sensors*, vol. 11, no. 7, pp. 6771–6798, 2011.
- [29] N. El-Sheimy, H. Hou, and X. Niu, "Analysis and modeling of inertial sensors using Allan variance," *IEEE Trans. Instrum. Meas.*, vol. 57, no. 1, pp. 140–149, Jan. 2008.
- [30] H. Carlsson, I. Skog, and J. Jalden, "Self-calibration of inertial sensor arrays," *IEEE Sensors J.*, vol. 21, no. 6, pp. 8451–8463, Mar. 2021.



**Liqiang Wang** received the B.Eng. (Hons.) degree in electronic information engineering from Wuhan University, Wuhan, China, in 2020, where he is currently pursuing the master's degree in navigation, guidance, and control with the GNSS Research Center. His primary research interests include GNSS/INS integrations and visual-based navigation.



**Hailiang Tang** received the B.Eng. and M.Eng. degrees from Wuhan University, China, in 2017 and 2020, respectively, where he is currently pursuing the Ph.D. degree in communication and information system with the GNSS Research Center. His current research interests include GNSS/INS integration technology, deep learning, visual SLAM, and autonomous robotic systems.



**Tisheng Zhang** received the B.Sc. and Ph.D. degrees in communication and information system from Wuhan University, Wuhan, China, in 2008 and 2013, respectively. He held a post-doctoral position at the Hong Kong Polytechnic University from 2017 to 2018. He is an Associate Professor with the GNSS Research Center, Wuhan University. His research interests focus on the fields of GNSS receiver and multi-sensor integrated navigation.



**Qijin Chen** received the B.Eng. and Ph.D. degrees in geodesy and survey engineering from Wuhan University, Wuhan, China, in 2011 and 2016, respectively. He is currently an Associate Researcher with the GNSS Research Center, Wuhan University. His research interests include INS with aiding and its applications in geodesy and precise surveying engineering, including railway track geometry measurement and underground pipeline surveying.



**Jinwei Shi** received the B.Eng. degree in electronic information engineering from Wuhan University, Wuhan, China, in 2020, where he is currently pursuing the master's degree in navigation, guide, and control with the GNSS Research Center. His primary research interest focuses on deeply-coupled GNSS receiver.



**Xiaoji Niu** received the bachelor's (Hons.) and Ph.D. degrees from the Department of Precision Instruments, Tsinghua University, in 1997 and 2002, respectively. He did postdoctoral research at the University of Calgary, Canada, and worked as a Senior Scientist at SiRF Technology Inc. He is a Professor with the GNSS Research Center, Wuhan University, Wuhan, China. Dr. Niu is currently leading the Integrated and Intelligent Navigation Group (i2Nav). He has published over 100 academic articles and holds more than 30 patents. His research focuses on GNSS/INS integration, low-cost navigation sensor fusion, and the relevant new applications.